Renewable Energy 64 (2014) 1–9

Contents lists available at ScienceDirect

Renewable Energy

journal homepage: www.elsevier.com/locate/renene

Review

The performance evaluation of unsteady MHD non-Darcy nanofluid flow over a porous wedge due to renewable (solar) energy

R. Kandasamy*, I. Muhaimin, A.K. Rosmila

Research Centre for Computational Mathematics, FSTPi, Universiti Tun Hussein Onn Malaysia, Batu Pahat, Johor, Malaysia

ARTICLE INFO

Article history:
Received 20 March 2013
Accepted 8 October 2013
Available online 16 November 2013

Keywords:
Nanofluid
Porous wedge
Unsteady non-Darcy flow
Magnetic field
Solar energy radiation

ABSTRACT

Solar energy has been used since the beginning of time and is vital to all living things. In addition to solar energy being a constant resource, heat and electricity are other forms of energy that can be made from solar energy. Technology allows solar energy to be converted into electricity through solar thermal heat. The main advantages of solar energy are that it is clean, able to operate independently or in conjunction with traditional energy sources, and is remarkably renewable. Nanofluid-based direct solar receivers, where nanoparticles in a liquid medium can scatter and absorb solar radiation, have recently received interest to efficiently distribute and store the thermal energy. The objective of the present work is to investigate theoretically the effect of copper nanoparticles in the presence of magnetic field on unsteady non-Darcy flow and heat transfer of incompressible copper nanofluid along a porous wedge due to solar energy. It is of special interest in this work to consider that the similarity transformation is used for unsteady flow. Copper nanofluid flow over a porous wedge plays a significant role and absorbs the incident solar radiation and transits it to the working fluid by convection.

1. Introduction

Energy plays an important role in the development of human society. However, over the past century, the fast development of human society leads to the shortage of global energy and the serious environmental pollution. All countries of the world have to explore new energy sources and develop new energy technologies to find the road to sustainable development. The sun is probably the most important source of renewable energy available today. Renewable energy sources which include solar energy (which comes from the sun and can be turned into electricity and heat), wind energy, geothermal energy (from inside the earth), biomass from plants, and hydropower from water are also renewable energy sources. Solar energy as the renewable and environmental friendly energy, it has produced energy for billions of years. Solar energy that reaches the earth is around 4×1015 MW, it is 2000 times as large as the global energy consumption. Thus the utilization of solar energy and the technologies of solar energy materials attract much more attention. Nano-material is a new energy material, since its particle size is the same as or smaller than the wavelength of de Broglie wave and coherent wave. Therefore, nanoparticle becomes to strongly absorb and selectively absorb incident radiation. Based on the radiative motion properties of nanoparticle, the utilization of nanofluids in solar thermal system becomes the new study hotspot. Scientists and engineers today seek to utilize solar radiation directly by converting it into useful heat or electricity.

The varieties of solar energy applications and advantages are enormous, scientists and engineers today seek to utilize solar radiation directly by converting it into useful heat or electricity. The inadequacy and inability and the inherent danger in the use of fossil fuels energy and other conventional sources of energy to meet the worlds demands for energy both now and in the nearest future is highlighted and emphasized. The world eventually turning to the renewable energy sources, solar energy in particular, is inevitable, expected and wise. The inevitable impediment such as the earth's atmosphere and its effect on the passage of solar radiation, to the realization of full utilization of solar energy are identified. Nano-material is a new energy material, since its particle size is the same as or smaller than the wavelength of de Broglie wave and coherent wave. Therefore, nanoparticle becomes to strongly absorb and selectively absorb incident radiation. Based on the radiation properties of nanoparticle, the utilization of nanofluids in solar thermal system becomes the new study hotspot. Radiative transport in porous media has important engineering applications in solar collectors and the porous medium acts as a means to absorb or emit radiant energy that is transferred to or from a fluid. Generally, the fluid itself can be assumed to be transparent to radiation, because the dimensions for radiative transfer among the solid structure

* Corresponding author. Tel.: +60 7 453 7416; fax: +60 7 453 6051.
E-mail address: future990@gmail.com (R. Kandasamy).

0960-1481/$ – see front matter © 2013 Elsevier Ltd. All rights reserved.
http://dx.doi.org/10.1016/j.renene.2013.10.019

elements of the porous medium are usually much less than the radiative mean free path for scattering or absorption in the fluid.

Solar energy is one of the best sources of renewable energy with minimal environmental impact, Angstrom [1] and Mostafa Keshavarz Moraveji and Majid Hejazian [2]. Power tower solar collectors could benefit from the potential efficiency improvements that arise from using a nanofluid as a working fluid. The basic concept of using particles to collect solar energy was studied in the 1970s by Hunt [3]. It has been shown that mixing nanoparticles in a liquid (nanofluid) has a dramatic effect on the liquid thermophysical properties such as thermal conductivity. Nanoparticles also offer the potential of improving the radiative properties of liquids, leading to an increase in the efficiency of direct absorption solar collectors. The study of heat transfer in the presence of nanofluids due to solar energy radiation is of great practical importance to engineers and scientists because of its almost universal occurrence in many branches of science and engineering. Numerous models and group theory methods have been proposed by different authors to study convective flows of nanofluids, e.g. Birkoff [4], Yurusoy and Pakdemirli [5] and Yurusoy et al. [6].

Convective flow in porous media has been widely studied in the recent years due to its wide applications in engineering as post-accidental heat removal in nuclear reactors, solar collectors, drying processes, heat exchangers, geothermal and oil recovery, building construction, etc. The effects of heat and mass transfer laminar boundary layer flow over a wedge have been studied by many authors (for example, Kafoussias and Nanousis [7], Kandasamy et al. [8] and Cheng and Lin [9]) in different situations. Nanofluids are suspensions of nanoparticles in fluids that show significant enhancement of their properties at modest nanoparticle concentration, which was investigated by Abdul-Kahar et al. [10], Kandasamy et al. [11], Vajravelu et al. [12] and Rana and Bhargava [13]. Nanofluids may be used in various applications which include electronic cooling, vehicle cooling transformer and coolant for nuclear reactors.

In this paper, we apply the so-called symmetry methods for a particular problem of fluid mechanics. The main advantage of such methods is that they can successfully be applied to nonlinear differential equations. The method of Lie group transformations is used to derive all group-invariant similarity solutions of the unsteady two-dimensional laminar boundary-layer equations. On the other hand, it is now well known that the classical Lie symmetry method can be used to find similarity solutions, invariants, integrals motion, etc. systematically, Ovsiannikov [14] and Avramenko et al. [15] analyzed the application of Lie group theory to the boundary layers. Solar energy is currently one kind of important resource for clean and renewable energy, and is widely investigated in many fields. For this reason, it is of special interest in this work to consider natural convection due to solar radiation non-Darcy flow from a wedge embedded in a porous medium with variable porosity distribution. The inertia effect is expected to be important at a higher flow rate and it can be accounted for through the addition of a velocity squared term in the momentum equation, which is known as the Forchheimer's extension. Several researchers have studied natural convection heat transfer in porous medium by considering Forchheimer's extension.

The motivation of the present study is to investigate the development of the unsteady non-Darcy boundary layer flow and heat transfer over a porous wedge sheet in a nanofluid due to solar radiation. Lie symmetry group transformation is utilized to convert the governing partial differential equations into ordinary differential equations and then the numerical solution of the problem is accomplished by using Runge Kutta Gill method [16] with shooting technique. This method has the following advantages over other available methods: (i) it utilizes less storage register (ii) it controls the growth of rounding errors and is usually stable and (iii) it is computationally economical. The analysis of the results obtained shows that the flow field is influenced appreciably by the presence of convective radiation and nanoparticles deposition in the presence of nanofluid past a porous wedge sheet.

2. Mathematical analysis

Let us consider an unsteady laminar two-dimensional non-Darcy flow of an incompressible viscous nanofluid past a porous wedge in the presence of solar energy radiation (see, Fig. 1). We consider influence of a constant magnetic field of strength B_0 which is applied normally to the sheet. The temperature at the wedge surface takes the constant value T_w, while the ambient value, attained as y tends to infinity, takes the constant value T_∞. Far away from the wedge plate, both the surroundings and the Newtonian, absorbing fluid are maintained at a constant temperature T_∞. It is further assumed that the induced magnetic field is negligible in comparison to the applied magnetic field (as the magnetic Reynolds number is small). The porous medium is assumed to be transparent and in thermal equilibrium with the fluid. The thermal dispersion effect is minimal when the thermal diffusivity of the porous matrix is of the same order of magnitude as that of the working fluid. This viewpoint of assuming that the effective thermal diffusivity remains constant when the porosity of the porous medium varies with the normal distance is shared by many other investigators such as Vafai et al. [17] and Tien and Hong [18]. The non reflecting absorbing ideally transparent wedge plate receives an incident radiation flux of intensity q''_{rad}. This radiation flux penetrates the plate and is absorbed in an adjacent fluid of absorption coefficient [19]. Due to heating of the absorbing nanofluid and the wedge plate by solar radiation, heat is transferred from the plate to the surroundings and the solar radiation is a collimated beam that is normal to the plate. The fluid is a water based nanofluid containing copper nanoparticles. As mentioned before, the working fluid is assumed to have heat absorption properties. For the present application, the porous medium absorbs the incident solar radiation and transits it to the working fluid by convection. The thermophysical properties of the nanofluid are given in Table 1 (see Ref. [20]). Under the above assumptions, the boundary layer equations governing the flow and thermal field can be written in dimensional form as

$$\frac{\partial \overline{u}}{\partial \overline{x}} + \frac{\partial \overline{v}}{\partial \overline{y}} = 0 \tag{1}$$

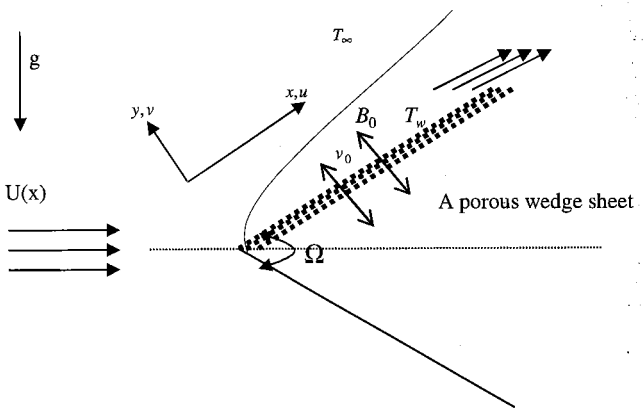

Fig. 1. Physical flow model over a porous wedge sheet.

Table 1
Thermophysical properties of fluid and nanoparticles.

	ρ (kg/m^3)	c_p (J/kg K)	k (W/mK)	$\beta \times 10^{-5}$ (K^{-1})
Pure water ($\zeta = 0.0$)	997.1	4179	0.613	21
Copper (Cu) ($\zeta = 0.05$)	8933	385	401	1.67
Silver (Ag) ($\zeta = 0.1$)	10,500	235	429	1.89
Alumina (Al_2O_3) ($\zeta = 0.15$)	3970	765	40	0.85
Titania (TiO_2) ($\zeta = 0.2$)	4250	6862	8.9538	0.9

$$\frac{\partial \overline{u}}{\partial \overline{t}} + \overline{u}\frac{\partial \overline{u}}{\partial \overline{x}} + \overline{v}\frac{\partial \overline{u}}{\partial \overline{y}} = \frac{1}{\rho_{f_n}}\left[\frac{\partial U}{\partial t}\rho_{f_n} + U\frac{dU}{dx}\rho_{f_n} + \mu_{f_n}\frac{\partial^2 \overline{u}}{\partial \overline{y}^2} + (\rho\beta)_{f_n}\overline{g}(T - T_\infty)\sin\frac{\Omega}{2} - \frac{F}{\sqrt{K}}\rho_{f_n}\left(\overline{u}^2 - U^2\right) - \left(\sigma B_0^2 + \frac{\nu_f}{K}\rho_{f_n}\right) \times (\overline{u} - U)\right] \tag{2}$$

$$\frac{\partial T}{\partial \overline{t}} + \overline{u}\frac{\partial T}{\partial \overline{x}} + \overline{v}\frac{\partial T}{\partial \overline{y}} = \alpha_{f_n}\frac{\partial^2 T}{\partial \overline{y}^2} - \frac{1}{(\rho c_p)_{f_n}}\frac{\partial q''_{rad}}{\partial y} + \frac{\mu_{f_n}}{(\rho c_p)_{f_n}}\left(\frac{\partial u}{\partial y}\right)^2 \tag{3}$$

Using Rosseland approximation for radiation [21] we can write $q''_{rad} = -(4\sigma_1\ 3k^*)(\partial T^4\ \partial y)$ where σ_1 is the Stefan–Boltzman constant is, k^* is the mean absorption coefficient. The Rosseland approximation is used to describe the radiative heat transfer in the limit of the optically thick fluid (nanofluid).

The boundary conditions of these equations are

$$\overline{u} = 0\quad \overline{v} = -v_0\quad T = T_w + c_1 x^{n_1}\ \text{at}\ \overline{y} = 0;\quad \overline{u}\ \ U = \frac{\nu_f x^m}{\delta^{m+1}}\quad T\quad T_\infty\ \text{as}\ \overline{y}\quad \infty \tag{4}$$

where c_1 and n_1 (power index) are constants and v_0 and T_w are the suction (0) or injection (0) velocity and the fluid temperature at the plate. Under this consideration, the potential flow velocity of the wedge can be written as $U(x\ t) = (\nu_f x^m)\ \delta^{m+1}$, $\beta_1 = (2m)\ (1 + m)$, where m is a constant (see in Ref. [22]) whereas δ is the time-dependent length scale which is taken to be (detailed in Sattar (1994) as: $\delta = \delta(t)$ and β_1 is the Hartree pressure gradient parameter that corresponds to $\beta_1 = \Omega\ \pi$ for a total angle Ω of the wedge, the temperature of the fluid is assumed to vary following a power-law function while the free stream temperature is linearly stratified. The suffixes w and ∞ denote surface and ambient conditions. Here $\overline{u}$ and $\overline{v}$ are the velocity components in the $\overline{x}$ and $\overline{y}$ directions, T is the local temperature of the nanofluid, $\overline{g}$ is the acceleration due to gravity, K is the permeability of the porous medium, F is the empirical constant in the second-order resistance and setting $F = 0$ in Equ. (2) is reduced to the Darcy law. v_0 is the velocity of suction/injection, K is the permeability of the porous medium, ρ_{f_n} is the effective density of the nanofluid, q''_{rad} is the applied absorption radiation heat transfer, μ_{f_n} is the effective dynamic viscosity of the nanofluid, α_{f_n} is the thermal diffusivity of the nanofluid which are defined as (see Ref. [23],

$$\rho_{f_n} = (1-\zeta)\rho_f + \zeta\rho_s \qquad \mu_{f_n} = \frac{\mu_f}{(1-\zeta)^{2.5}}$$

$$(\rho\beta)_{f_n} = (1-\zeta)(\rho\beta)_f + \zeta(\rho\beta)_s \qquad \alpha_{f_n} = \frac{k_{f_n}}{(\rho c_p)_{f_n}}$$

$$(\rho c_p)_{f_n} = (1-\zeta)(\rho c_p)_f + \zeta(\rho c_p)_s$$

Maxwell [24] model was developed to determine the effective electrical or thermal conductivity of liquid–solid suspensions. This model is applicable to statistically homogeneous and low volume concentration liquid–solid suspensions, with randomly dispersed and uniformly sized non-contacting spherical particles. It is given as:

$$\frac{k_{f_n}}{k_f} = \left\{\frac{\left(k_s + 2k_f\right) - 2\zeta\left(k_f - k_s\right)}{\left(k_s + 2k_f\right) + 2\zeta\left(k_f - k_s\right)}\right\} \tag{5}$$

Experiments report thermal conductivity enhancement of nanofluids beyond the Maxwell limit of 3ζ. In the limit of low particle volume concentration (ζ) and the particle conductivity (k_s), being much higher than the base liquid conductivity (k_f), Equ. (5) can be reduced to Maxwell 3ζ limit as:

$$k_{low} = \frac{k_{f_n}}{k_f} = 1 + 3\zeta \tag{5a}$$

Equation (5) represents the lower limit for the thermal conductivity of nanofluids and it can seen that in the limit where $\zeta = 0$ (no particles), Equ. (5a) yields $k_{low} = 1$ as expected. Where k_f and k_s are the thermal conductivity of the base fluid and nanoparticle respectively, ζ is the nanoparticle volume fraction, μ_f is the dynamic viscosity of the base fluid, β_f and β_s are the thermal expansion coefficients of the base fluid and nanoparticle, respectively, ρ_f and ρ_s are the density of the base fluid and nanoparticle, respectively, k_{f_n} is the effective thermal conductivity of the nanofluid and $(\rho c_p)_{f_n}$ is the heat capacitance of the nanofluid.

By introducing the following non-dimensional variables

$$x = \frac{\overline{x}}{\sqrt{\frac{\nu_f}{c}}}\quad y = \frac{\overline{y}}{\sqrt{\frac{\nu_f}{c}}}\quad u = \frac{\overline{u}}{\sqrt{c\nu_f}}\quad v = \frac{\overline{v}}{\sqrt{c\nu_f}}\ \text{and}\ \theta = \frac{T - T_\infty}{T_w - T_\infty} \tag{6}$$

Equations (1)–(4) take the non-dimensional form

$$\frac{\partial u}{\partial x} + \frac{\partial v}{\partial y} = 0 \tag{7}$$

$$\frac{\partial u}{\partial t} + u\frac{\partial u}{\partial x} + v\frac{\partial u}{\partial y} = \frac{1}{\left(1 - \zeta + \zeta\frac{\rho_s}{\rho_f}\right)}\left[\left\{\frac{\partial U}{\partial t} + U\frac{dU}{dx} - \frac{F}{\sqrt{K}}\left(u^2 - U^2\right)\right\} \times \frac{\rho_{f_n}}{\rho_f} + \frac{\nu_f}{(1-\zeta)^{2.5}}\frac{\partial^2 u}{\partial y^2} + \left\{\left(1 - \zeta + \zeta\frac{(\rho\beta)_s}{(\rho\beta)_f}\right)\gamma\sin\frac{\Omega}{2}\theta\right\} - \left(\frac{\sigma B_0^2}{\rho_f} + \frac{\nu_f}{K(1-\zeta)^{2.5}}\right)(u - U)\right] \tag{8}$$

$$\frac{\partial T}{\partial t} + u\frac{\partial T}{\partial x} + v\frac{\partial T}{\partial y} = \frac{1}{1 - \zeta + \zeta\frac{(\rho c_p)_s}{(\rho c_p)_f}}\left[\frac{1}{Pr_f}\left\{\frac{k_{f_n}}{k_f}\frac{\partial^2 T}{\partial y^2} + \frac{4}{3}N\left((C_T + \theta)^3\theta'\right)' + \frac{\mu_{f_n}}{(\rho c_p)_f}\left(\frac{\partial u}{\partial y}\right)^2\right\}\right] \tag{9}$$

with the boundary conditions

$$\bar{u} = 0,\ \bar{v} = -V_0,\ T = T_w \text{ at } \bar{y} = 0$$
$$\bar{u} \quad U = \frac{\nu_f x^m}{\delta^{m+1}},\ T \quad T_\infty \text{ as } \bar{y} \quad \infty \tag{10}$$

where $Pr_f = \nu_f/\alpha_f$ is the Prandtl number, $\lambda = \delta^{m+1}/(Kk^2)$ is the porous media parameter, $\gamma = (g(\rho\beta)_f\Delta T)/\left(\rho_f U^2 k^{\frac{2}{1-m}}\right)$ is the buoyancy or natural convection parameter, $N = (4\sigma_1\theta_w^3)/(k_f k^*)$ is the conductive radiation parameter, $F_n = (\xi/k)^{\frac{2}{1-m}}(F/\sqrt{K})$ Forchheimer number, $Ec = (\mu_f/(\rho c_p)_f)(U^2/(T_w - T_\infty))$ is the Eckert number, $M = (\sigma B_0^2/\mu_f)(\delta^{m+1}/k^2)$ is the magnetic parameter and $C_T = T_\infty/(T_w - T_\infty)$ is the temperature ratio where C_T assumes very small values by its definition as $T_w - T_\infty$ is very large compared to T_∞. In the present study, it is assigned the value 0.1. It is worth mentioning that $\gamma > 0$ aids the flow and $\gamma < 0$ opposes the flow, while $\gamma = 0$ i.e., $(T_w - T_\infty)$ represents the case of forced convection flow. On the other hand, if γ is of a significantly greater order of magnitude than one, then the buoyancy forces will be predominant. Hence, combined convective flow exists when $\gamma = O(1)$.

Following the lines of Kafoussias and Nanousis [7], the changes of variables are

$$\eta = y\sqrt{\frac{(1+m)}{2}}\sqrt{\frac{x^{m-1}}{\delta^{m+1}}},\ \psi = \sqrt{\frac{2}{1+m}}\,\frac{\nu_f x^{\frac{m+1}{2}}}{\delta^{\frac{m+1}{2}}} f(\eta) \text{ and}$$
$$\theta = \frac{T - T_\infty}{T_w - T_\infty} \tag{11}$$

By introducing the stream function ψ, which defined as $u = \partial\psi/\partial y$ and $v = -\partial\psi/\partial x$, then the system of equations (7)–(9) become

$$\frac{\partial^2\psi}{\partial t\partial y} + \frac{\partial\psi}{\partial y}\frac{\partial^2\psi}{\partial x\partial y} - \frac{\partial\psi}{\partial x}\frac{\partial^2\psi}{\partial y^2} = \frac{1}{\left(1-\zeta+\zeta\frac{\rho_s}{\rho_f}\right)}\left[\left\{\left(1-\zeta+\zeta\frac{(\rho\beta)_s}{(\rho\beta)_f}\right)\right.\right.$$
$$\left.\times\gamma\sin\frac{\Omega}{2}\theta\right\} + \frac{1}{(1-\zeta)^{2.5}}\frac{\partial^3\psi}{\partial y^3} + \left\{\frac{\partial U}{\partial t} + U\frac{dU}{dx} - \frac{F}{\sqrt{K}}\left(\left(\frac{\partial\psi}{\partial y}\right)^2 - U^2\right)\right\}$$
$$\left.\times\frac{\rho_{f_n}}{\rho_f} - \left(\frac{\sigma B_0^2}{\rho_f} + \frac{\nu_f}{K(1-\zeta)^{2.5}}\right)\left(\frac{\partial\psi}{\partial y} - U\right)\right] \tag{12}$$

$$\frac{\partial\theta}{\partial t} + \frac{\partial\psi}{\partial y}\frac{\partial\theta}{\partial x} - \frac{\partial\psi}{\partial x}\frac{\partial\theta}{\partial y} = \frac{1}{1-\zeta+\zeta\frac{(\rho c_p)_s}{(\rho c_p)_f}}\left[\frac{1}{Pr_f}\left\{\frac{k_{f_n}}{k_f}\frac{\partial^2\theta}{\partial y^2}\right.\right.$$
$$\left.\left. + \frac{4}{3}N\left((C_T+\theta)^3\theta'\right)' + \frac{\mu_{f_n}}{(\rho c_p)_f}\left(\frac{\partial^2\psi}{\partial y^2}\right)^2\right\}\right] \tag{13}$$

with the boundary conditions

$$\frac{\partial\psi}{\partial y} = 0,\ \frac{\partial\psi}{\partial x} = -V_0,\ T = T_w \text{ at } y = 0$$
$$\frac{\partial\psi}{\partial y} \quad \frac{\nu_f x^m}{\delta^{m+1}},\ T \quad T_\infty \text{ as } \bar{y} \quad \infty \tag{14}$$

The symmetry groups of Equs. (12) and (13) are calculated using classical Lie group approach (see Ref. [11]). With the help of these relations, the (12) and (13) become

$$f''' - \frac{\frac{2}{m+1}(1-\zeta)^{2.5}\xi^2}{\left(1-\zeta+\zeta\frac{\rho_s}{\rho_f}\right)}\left[\left(M + \frac{\lambda}{(1-\zeta)^{2.5}}\right)(f'-1)\right.$$
$$-\xi^{\frac{1}{1-m}}\left\{1-\zeta+\zeta\frac{(\rho c_p)_s}{(\rho c_p)_f}\right\}\gamma\sin\frac{\Omega}{2}\theta\Bigg] - \left(1-\zeta+\zeta\frac{\rho_s}{\rho_f}\right)(1-\zeta)^{2.5}$$
$$\times\left[\frac{2}{m+1}(m-F_n)\left(f'^2-1\right) - ff'' + \lambda_u(2-\eta f'' - 2f')\right.$$
$$\left.+\frac{1-m}{1=m}\xi\frac{\partial f}{\partial\xi}\left(\frac{\partial f}{\partial\eta} - \frac{\partial^2 f}{\partial\eta^2}\right)\right] = 0 \tag{15}$$

$$\theta'' + \frac{4}{3}\frac{k_f}{k_{f_n}}N\left\{(C_T+\theta)^3\theta'\right\}' + \frac{Pr_f}{(1-\zeta)^{2.5}}Ec(f'')^2$$
$$-Pr_f\left\{1-\zeta+\zeta\frac{(\rho c_p)_s}{(\rho c_p)_f}\right\}\frac{k_f}{k_{f_n}}\left[\frac{2n_1}{m+1}f'\theta - f\theta' + \lambda_v\eta\theta'\right. \tag{16}$$
$$\left.+\frac{1-m}{1+m}\left\{\xi\frac{\partial\theta}{\partial\xi}\frac{\partial f}{\partial\eta} - \xi\frac{\partial f}{\partial\xi}\frac{\partial\theta}{\partial\eta}\right\}\right] = 0$$

The boundary conditions take the following form

$$\frac{\partial f}{\partial\eta} = 0,\ \frac{m+1}{2}f + \frac{1-m}{2}\xi\frac{\partial f}{\partial\xi} = -S,\ \theta = 1 \text{ at } \eta = 0 \text{ and}$$
$$\frac{\partial f}{\partial\eta} = 1,\ \theta \quad 0 \text{ as } \eta \quad \infty \tag{17}$$

where S is the suction parameter if $S > 0$ and injection if $S < 0$ and $\xi = kx^{(1-m)/2}$ [7] is the dimensionless distance along the wedge ($\xi > 0$). In this system of equations, it is obvious that the non-similarity aspects of the problem are embodied in the terms containing partial derivatives with respect to ξ. This problem does not admit similarity solutions. Thus, with ξ-derivative terms retained in the system of equations, it is necessary to employ a numerical scheme suitable for partial differential equations for the solution. Formulation of the system of equations for the local nonsimilarity model with reference to the present problem will now be discussed.

At the first level of truncation, the terms accompanied by $\xi(\partial/\partial\xi)$ are small. This is particularly true when ($\xi \ll 1$). Thus the terms with $\xi(\partial/\partial\xi)$ on the right-hand sides of Equations (20) and (21) are deleted to get the following system of equations:

$$f''' - \frac{\frac{2}{m+1}(1-\zeta)^{2.5}\xi^2}{\left(1-\zeta+\zeta\frac{\rho_s}{\rho_f}\right)}\left[\left(M + \frac{\lambda}{(1-\zeta)^{2.5}}\right)(f'-1)\right.$$
$$-\xi^{\frac{1}{1-m}}\left\{1-\zeta+\zeta\frac{(\rho c_p)_s}{(\rho c_p)_f}\right\}\gamma\sin\frac{\Omega}{2}\theta\Bigg] - \left(1-\zeta+\zeta\frac{\rho_s}{\rho_f}\right)(1-\zeta)^{2.5}$$
$$\left.\times\left[\frac{2}{m+1}(m-F_n)\left(f'^2-1\right) - ff'' + \lambda_u(2-\eta f'' - 2f')\right]\right. = 0 \tag{18}$$

$$\theta'' + \frac{4}{3}\frac{k_f}{k_{f_n}}N\left\{(C_T+\theta)^3\theta'\right\}' + \frac{Pr_f}{(1-\zeta)^{2.5}}Ec(f'')^2$$
$$-Pr_f\left\{1-\zeta+\zeta\frac{(\rho c_p)_s}{(\rho c_p)_f}\right\}\frac{k_f}{k_{f_n}}\left[\frac{2n_1}{m+1}f'\theta - f\theta' + \lambda_v\eta\theta'\right] = 0 \tag{19}$$

The boundary conditions take the following form

$$f' = 0,\ f = -\frac{2S}{m+1},\ \theta = 1 \text{ at } \eta = 0 \text{ and } f' = 1,\ \theta \to 0 \text{ as } \eta \to \infty \tag{20}$$

Further, we suppose that $\lambda_v = c/x^{m-1}$ where c is a constant so that $c = (\delta^m/\nu_f)(d\delta/dt)$ and integrating, it is obtained that $\delta = [c(m+1)\nu_f t]^{1/(m+1)}$. When $c = 2$ and $m = 1$ in δ and we get $\delta = 2\sqrt{\nu_f t}$ which shows that the parameter δ can be compared with the well established scaling parameter for the unsteady boundary layer problems (see Ref. [25]).

For practical purposes, the functions $f(\eta)$ and $\theta(\eta)$ allow us to determine the skin friction coefficient

$$C_f = \frac{\mu_{f_n}}{\rho_f U^2}\left(\frac{\partial u}{\partial y}\right)_{\text{at } y=0} = -\frac{1}{(1-\zeta)^{2.5}}(Re_x)^{-\frac{1}{2}} f''(0) \tag{21}$$

and the Nusselt number

$$Nu_x = \frac{x k_{f_n}}{k_f(T_w - T_\infty)}$$
$$\left(\frac{\partial T}{\partial y}\right)_{\text{at } y=0} = -(Re_x)^{\frac{1}{2}}\frac{k_{f_n}}{k_f}\theta'(0)\left[1 + \frac{4}{3}N(C_T + \theta(0))^3\right] \tag{22}$$

respectively. Here, $Re_x = Ux/\nu_f$ is the local Reynolds number.

The set of Equs. (18) and (19) are highly nonlinear and coupled, and therefore, it cannot be solved analytically. Therefore, the nonlinear systems consisting of Equs. (18) and (19) along with the boundary conditions (20) have been solved numerically by applying Runge–Kutta-Gill [16] integration scheme together with shooting iteration technique(see also Ref. [8]) with Pr_f, ζ, λ, n_1, λ_v, S, Ω, M, F_n and N as prescribed parameters. A step size of $\Delta\eta = 0.01$ was selected to be satisfactory for a convergence criterion of 10^{-6} in all cases. The case $\gamma \gg 1.0$ corresponds to pure free convection, $\gamma = 1.0$ corresponds to mixed convection and $\gamma \ll 1.0$ corresponds to pure forced convection. Throughout this calculation we have considered $\gamma = 2.0$ unless otherwise specified. In order to validate our method, we have compared the results of $f(\eta)$, $f'(\eta)$ and $f''(\eta)$ for various values of η (Table 2) with those of White [26] whereas $f''(0)$ and $\theta'(0)$ for various values of ζ (Table 3) with those of Vajravelu et al. [12] and found them in excellent agreement.

In order to ascertain the accuracy of our numerical results, the present study is compared with the available exact solution in the literature. The velocity profiles for different values of m are compared with the available exact solution of Ref. [25], is shown in Fig. 2. It is observed that the agreement with the theoretical solution of velocity profile is excellent.

Table 2
Comparison of the current results with previous published work for $f(\eta)$, $f'(\eta)$ and $f''(\eta)$.

η	White [26]			Present works		
	$f(\eta)$	$f'(\eta)$	$f''(\eta)$	$f(\eta)$	$f'(\eta)$	$f''(\eta)$
0.0	0.000000	0.000000	0.469599	0.000000	0.000000	0.469686
0.5	0.05864	0.23423	0.46503	0.058656	0.234267	0.465078
1.0	0.23299	0.46063	0.43438	0.232986	0.460628	0.434377
2.0	0.88680	0.81669	0.25567	0.886797	0.816687	0.255668
3.0	1.79557	0.96905	0.06771	1.795569	0.969046	0.067714
4.0	2.78388	0.99777	0.00687	2.783882	0.997773	0.006871

Table 3
Comparison of the current results with previous published work for $f''(0)$ and $\theta'(0)$.

γ	ζ	Vajravelu et al. [12]		Present works	
		$f''(0)$	$\theta'(0)$	$f''(0)$	$\theta'(0)$
0.0	0.0	−1.001411	−2.972286	−1.00141137	−2.97228562
0.0	0.1	−1.175203	−2.476220	−1.17520279	−2.47622035
0.0	0.2	−1.218301	−2.094192	−1.21830078	−2.09419169

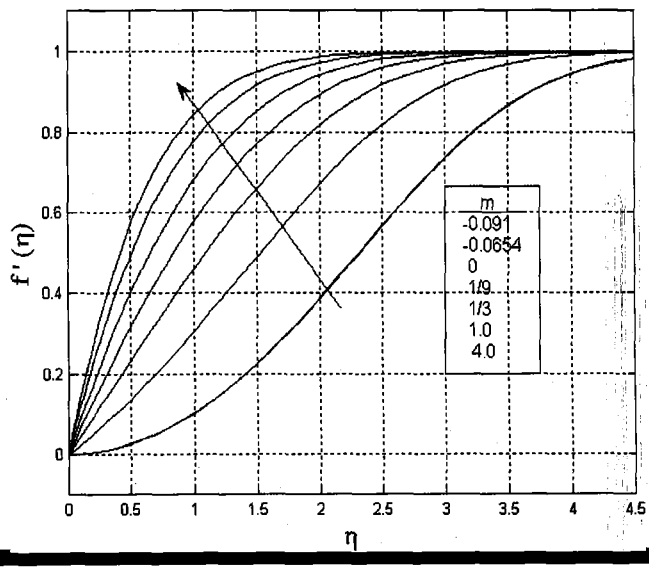

Fig. 2. Effects of m on the velocity distribution in the laminar flow past a wedge.

Figs. 3 and 4 present typical profiles for temperature for different values of magnetic parameter in the case of pure water and Cu–water (nanofluid). Due to the uniform convective radiation, it is clearly shown that the above mentioned two cases, the temperature of the fluid accelerates with increase of the strength of magnetic field, which implies that the applied magnetic field tends to heat the fluid and enhances the heat transfer from the wall. As it

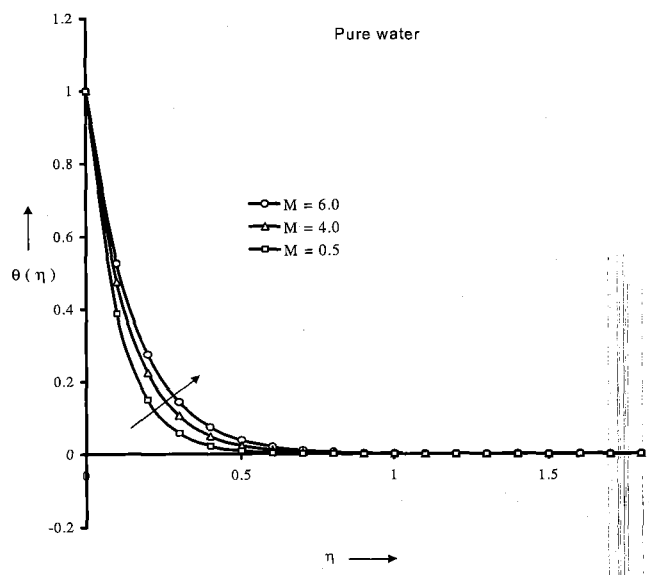

Fig. 3. Temperature profiles for various values of M (Pure water) ($\zeta = 0.00$, $\lambda_v = 0.1$, $N = 0.5$ and $m = 0.0909$ ($\Omega = 30°$)).

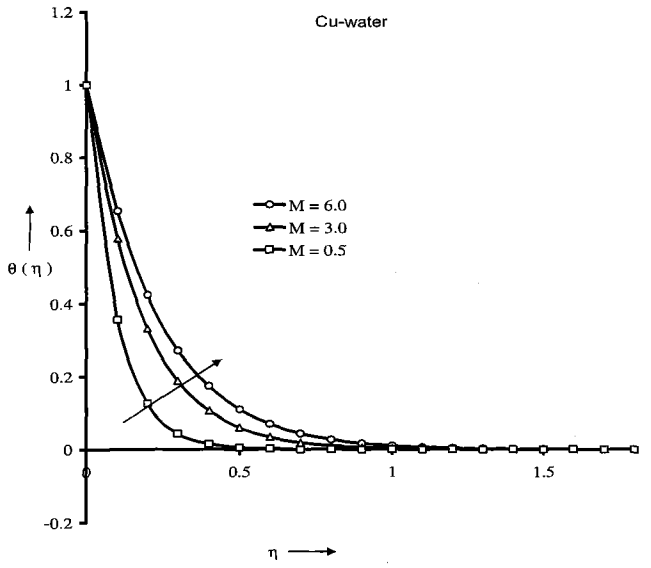

Fig. 4. Temperature profiles for various values of M (Cu–water) ($\zeta = 0.05$, $\lambda_v = 0.1$, $N = 0.5$ and $m = 0.0909$ ($\Omega = 30°$)).

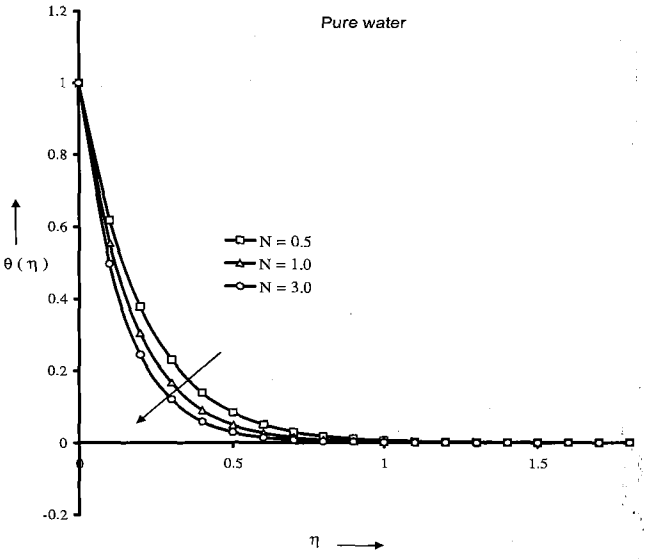

Fig. 6. Effects of convective radiation over temperature profiles (Pure water) ($\zeta = 0.00$, $\lambda_v = 0.1$, $M = 1.0$ and $m = 0.0909$ ($\Omega = 30°$)).

moves away from the plate, the effect of M becomes less pronounced. The effects of a transverse magnetic field to an electrically conducting fluid gives rise to a resistive-type force called the Lorentz force. This force clearly indicates that the transverse magnetic field opposes the transport phenomena and it has the tendency to slow down the motion of the fluid and to accelerate its temperature profiles. In all cases, the temperature vanishes at some large distance from the surface of the wedge. This result qualitatively agrees with the expectations, since magnetic field exerts retarding force on the natural convection flow. Physically, it is interesting to note that the temperature of the nanofluid (Cu Water) increases significantly as compared to that of the base fluid, because the copper Cu has high thermal conductivity. Magnetic nanofluid is a unique material that has both the liquid and magnetic properties. Many of the physical properties of these fluids can be tuned by varying magnetic field. These results clearly demonstrate that the magnetic field can be used as a means of controlling the flow and heat transfer characteristics.

Fig. 5 illustrates the effect of nanoparticle volume fraction ζ on the nanofluid temperature profile. It is clear that as the nanoparticle volume fraction increases, the nanofluid temperature increases and tends asymptotically to zero as the distance increases from the boundary. Increasing the volume fraction of nanoparticles increases the thermal conductivity of the nanofluid and we predict a thickening of the thermal boundary layer. We also observe that the temperature distribution in Silver–water and Alumina–water nanofluids are higher than that of Cu–water nanofluid. It is observed that with increasing ζ, the thermal boundary layer thickness increases. The sensitivity of thermal boundary layer

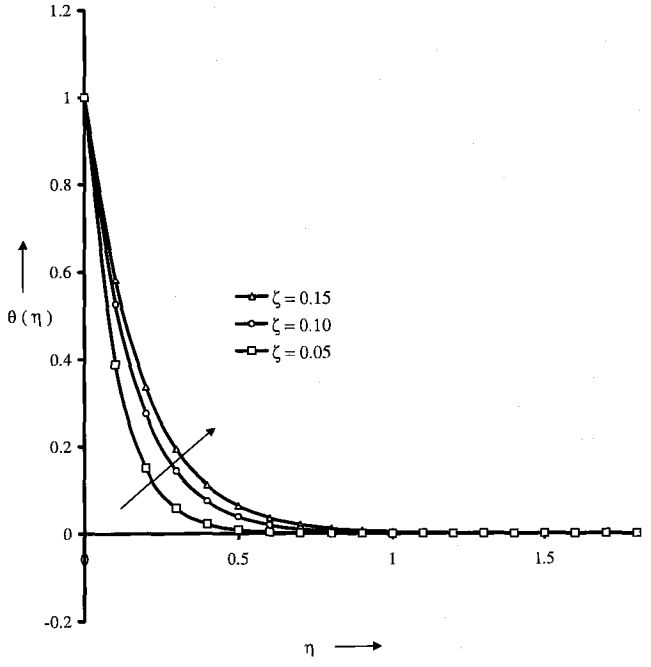

Fig. 5. Temperature profiles for various values of ζ ($N = 0.5$, $\lambda_v = 0.1$, $M = 1.0$ and $m = 0.0909$ ($\Omega = 30°$)).

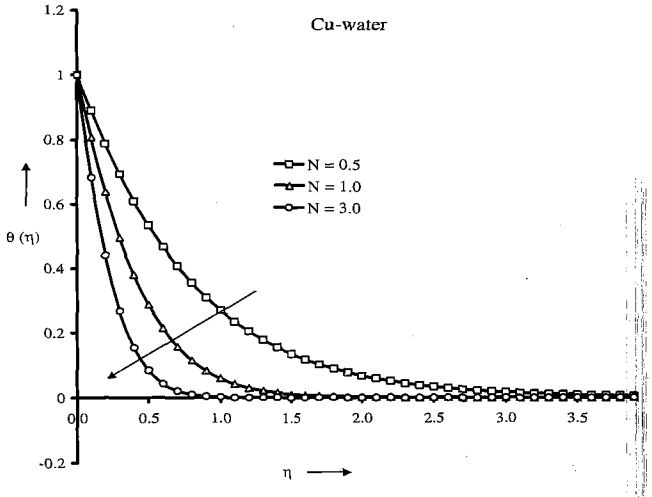

Fig. 7. Effects of convective radiation over temperature profiles (Cu–water) ($\zeta = 0.05$, $\lambda_v = 0.1$, $M = 1.0$ and $m = 0.0909$ ($\Omega = 30°$)).

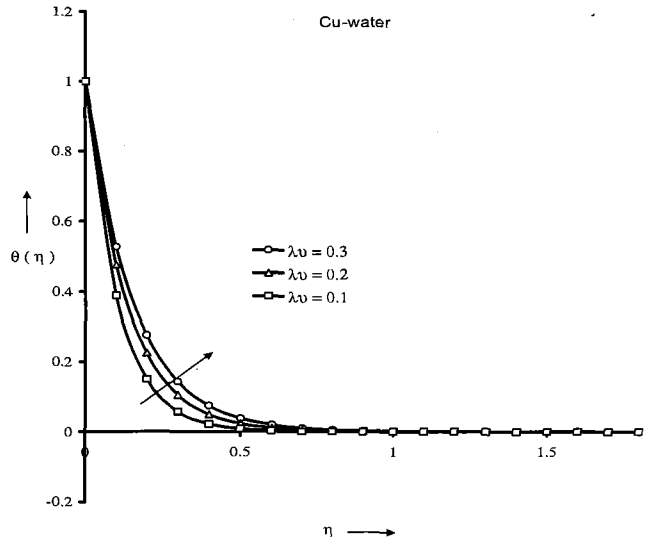

Fig. 8. Temperature profiles for various values of unsteadiness parameter (ζ = 0.05, N = 0.5, M = 1.0 and m = 0.0909 (Ω = 30°)).

thickness with ζ is related to the increased thermal conductivity of the nanofluid. In fact, higher values of thermal conductivity are accompanied by higher values of thermal diffusivity. The high value of thermal diffusivity causes a drop in the temperature gradients and accordingly increases the boundary thickness as demonstrated in Fig. 5. This agrees with the physical behavior, when the volume of copper nanoparticles increases the thermal conductivity increases, and then the thermal boundary layer thickness increases. Changes in the size, shape, material and volume fraction of the nanoparticles allow for tuning to maximize spectral absorption of solar energy throughout the fluid volume because the nanoparticle volume fraction parameter depends on the size of the particles. Enhancement in thermal conductivity can lead to efficiency improvements, although small, via more effective fluid heat transfer. In convective heat transfer in nanofluids, the heat transfer depends not only on the thermal conductivity but also on other properties, such as the specific heat, density, and dynamic viscosity of a nanofluid. Based on the experimental data [27]. Utilization of nanofluid instead of conventional base fluids results in remarkable heat transfer enhancement. In straight tubes heat transfer rate goes up as the nanoparticle mass concentration increases. Besides, nanofluid flows showed much higher Nusselt numbers compared to the base fluid flow. Finally, it was observed that combination of the two enhancing methods has a noticeably high capability to the heat transfer rate.

Figs. 6 and 7 present the characteristic temperature profiles for different values of the convective radiation parameter N in the presence of base fluid (pure water) and nanofluid (Cu–water). In both the cases, it is noticed that the temperature decelerates with increase of the radiation parameter N. According to Equations (2) and (3), the divergence of the radiative heat flux increases as thermal conductivity of the fluid decreases which in turn increases the rate of radiative heat transferred to the nanofluid and hence the fluid temperature decreases. The effect of radiation is to decrease the rate of energy transport to the fluid, thereby decreasing the temperature of the fluid. In view of this explanation, the effect of convective radiation becomes more significant as N 0 ($N \neq 0$) and can be neglected when N . This is because the large values correspond to an increased dominance of conduction over radiation thereby decreasing buoyancy force and thickness of the thermal boundary layer, despite of improved thermal conductivity for specific volume concentration of copper nanoparticles. Further, it is observed that the temperature of the Cu-nanofluid is decelerated significantly as compared to that of the base fluid. It should be noted that the enhancement of heat transfer greatly depends on particle type, particle size, base fluid, flow regime and specially boundary condition. The presence of nanoparticles in fluid changes the flow structure so that besides of thermal conductivity increment, chaotic movements, dispersions and fluctuations of nanoparticles especially near the wall leads to increase in the energy exchange rates and augments heat transfer rate between the fluid and the wall. This is in agreement with the physical fact that the thermal boundary layer thickness decreases with increasing radiation parameter N.

The effects of unsteadiness parameter λ_υ on the dimensionless temperature profiles within the nanofluid boundary-layer have been displayed in Fig. 8. It is observed that the temperature of the

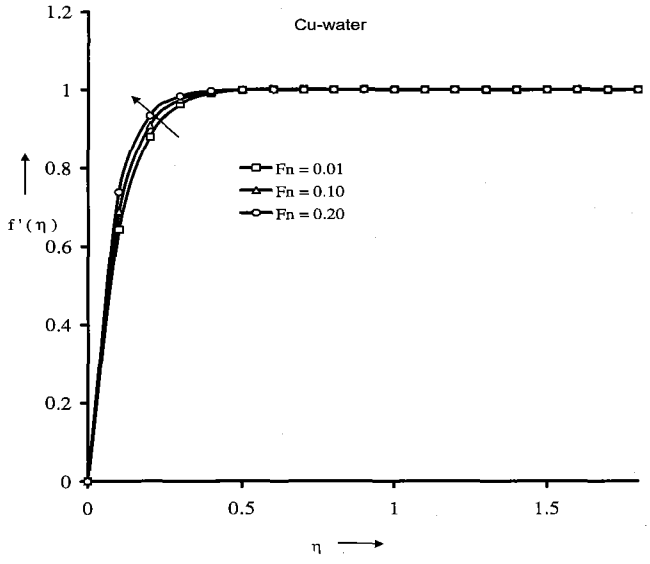

Fig. 9. Forchheimer number over the velocity profiles (ζ = 0.05, λ_υ = 0.1, N = 0.5 and m = 0.0909 (Ω = 30°)).

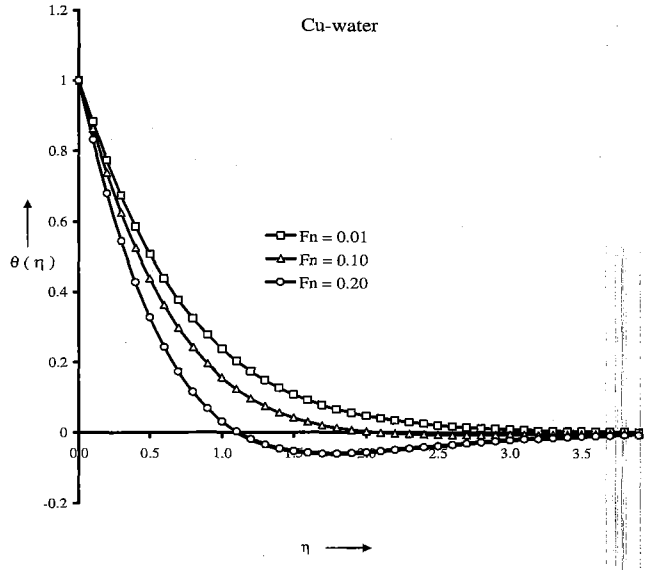

Fig. 10. Forchheimer number over the temperature profiles (ζ = 0.05, λ_υ = 0.1, N = 0.5 and m = 0.0909 (Ω = 30°)).

nanofluid increases with the increase of unsteadiness parameter λ_v and also it is found to decrease with the increase of η. The variation of the Prandtl number within the boundary layer for different values of the unsteadiness parameter λ_v plays a dominant role on nanofluid flow field. Significant change in the rate of decrease of θ for increasing values of λ_v is noticed. Temperature at a point on the sheet decreases significantly with the increase in λ_v i.e. rate of heat transfer increases with increasing unsteadiness parameter λ_v. The reason for this behavior is that the inertia of the porous medium provides an additional resistance to the fluid flow mechanism, which causes the fluid to move at a retarded rate with reduced velocity.

Figs. 9 and 10 illustrate typical profiles for velocity and temperature for different values of inertial parameter F_n in the case of Cu–water. In the presence of uniform magnetic field, it is clearly shown that the velocity increases and temperature decreases as the inertial parameter (Forchheimer number) increases. In particular, the velocity of the Cu-nanofluid increases whereas the temperature of the fluid gradually changes from higher value to the lower value only when the strength of inertial parameter F_n is higher than the nanoparticle volume fraction parameter. For heat transfer characteristics mechanism, interesting result is the large distortion of the temperature field caused for 0 05 $F_n \leq$ 0 5. The nanofluid becomes unstable and has no physical application at solid volume fractions greater than 0.05. In the case of Cu–water, negative value of the temperature profile is seen in the outer boundary region for F_n = 0 1 and 0 2. Non-Darcy behavior is important for describing fluid flow in porous media in situations where high velocity occurs. This is consistent with the fact that non-Darcy behavior is more severe in low permeability porous media. All these physical behavior are due to the combined effects of the strength of volume fraction of the nanoparticles in the presence of non-Darcy flow.

4. Conclusions

In this work, the effect of copper nanoparticles in the presence of magnetic field on unsteady non-Darcy flow and heat transfer of incompressible copper nanofluid along a porous wedge due to solar energy have been analyzed. It is of special interest in this work to consider the similarity transformation is used for unsteady flow.

1. Thermal boundary layer thickness of copper nanofluid is stronger than that of the base fluid as the strength of the magnetic field increases because the driving force to the nanofluid decreases as a result of temperature profiles increase.
2. It is noticed that the temperature of a nanofluid is decelerated significantly as compared to that of the base fluid with increase of convective radiation.
3. It has been shown that mixing nanoparticles in a liquid (nanofluid) has a dramatic effect on the liquid thermophysical properties such as thermal conductivity. It implies that the thermal conductivity of nanofluid is strongly dependent on the nanoparticle volume fraction.
4. Increase of thermal boundary layer field due to increase in nanoparticle volume fraction and magnetic parameters show that the temperature decreases gradually as we replace Copper nanofluid, ζ = 0 05 by Silver, ζ = 0 10 and Alumina nanofluid, ζ = 0 15 in the said sequence.
5. It is seen that the temperature of the nanofluid increases with the increase of unsteady parameter.
6. In the presence of uniform magnetic field, it is clearly shown that the velocity increases and temperature decreases as the inertial parameter (Forchheimer number) increases.
7. Copper nanofluid flow over a porous wedge plays a significant role and absorbs the incident solar radiation and transits it to the working fluid by convection.

The impact of nanoparticles on the absorption of radiative energy has been of interest for many years for a variety of applications. More recently researchers have become interested in the radiative properties of nanoparticles in liquid suspensions especially for medical and other engineering applications. Besides the benefits to the optical and radiative properties, nanofluids provide other benefits such as increased thermal conductivity and particle stability over micron-sized suspensions, which provide potential improvements to the operating efficiency of a direct absorption solar collector. Nanofluids have been shown to possess improved heat transport properties and higher energy efficiency in a variety of thermal exchange systems for different industrial applications, such as transportation, electronic cooling, military, nuclear energy, aerospace etc. Nanofluids due to solar energy are important because they can be used in numerous applications involving heat transfer and other applications such as in detergency, solar collectors, drying processes, heat exchangers, geothermal and oil recovery, building construction, etc.

References

[1] Angstrom AK. Solar and atmospheric radiation. J Roy Meteorol Soc 1924;50:121–6.
[2] Moraveji Mostafa Keshavarz, Hejazian Majid. Modeling of turbulent forced convective heat transfer and friction factor in a tube for Fe_3O_4 magnetic nanofluid with computational fluid dynamics. Int Commun Heat Mass Transfer 2012;39:1293–6.
[3] Hunt AJ. Small particle heat exchangers. J Renew Sustain Energy 1978. Lawrence Berkeley laboratory report no. LBL-7841.
[4] Birkoff G. Hydrodynamics. New Jersey: Princeton University Press; 1960.
[5] Yurusoy M, Pakdemirli M. Exact solutions of boundary layer equations of a special non-Newtonian fluid over a stretching sheet. Mech Res Commun 1999;26:171–5.
[6] Yurusoy M, Pakdemirli M, Noyan OF. Lie group analysis of creeping flow of a second grade fluid. Int J Non-linear Mech 2001;36:955–60.
[7] Kafoussias NG, Nanousis ND. Magnetohydrodynamic laminar boundary layer flow over a wedge with suction or injection. Canad J Phys 1997;75:733–41.
[8] Kandasamy R, Muhaimin I, Hashim Ishak, Ruhaila. Thermophoresis and chemical reaction effects on non-Darcy mixed convective heat and mass transfer past a porous wedge with variable viscosity in the presence of suction or injection. Nucl Eng Design 2008;238:2699–705.
[9] Cheng WT, Lin HT. Non-similarity solution and correlation of transient heat transfer in laminar boundary layer flow over a wedge. Int J Eng Sci 2002;40:531–40.
[10] Abdul Kahar Rosmila, Kandasamy R, Muhaimin I. Scaling group transformation for boundary-layer of a nanofluid past a porous vertical stretching surface in the presence of chemical reaction with heat radiation. Comput Fluids 2011;52:15–21.
[11] Kandasamy R, Loganathan P, Puvi Arasu P. Scaling group transformation for MHD boundary-layer flow of a nanofluid past a vertical stretching surface in the presence of suction/injection. Nucl Eng Design 2011;241:2053–9.
[12] Vajravelu K, Prasad KV, Lee Jinho, Lee Changhoon, Pop I, Van Gorder Robert A. Convective heat transfer in the flow of viscous Ag–water and Cu–water nanofluids over a stretching surface. Int J Therm Sci 2011;50:843–51.
[13] Rana R, Bhargava R. Numerical study of heat transfer enhancement in mixed convection flow along a vertical plate with heat source/sink utilizing nanofluids. Commun Nonlin Sci Numer Simul 2011;16:4318–34.
[14] Ovsiannikov LV. Group analysis of differential equations. New York: Academic Press; 1982.
[15] Avramenko AA, Kobzar SG, Shevchuk IV, Kuznetsov AV, Iwanisov LT. Symmetry of turbulent boundary layer flows: investigation of different eddy viscosity models. Acta Mech 2001;151:1–14.
[16] Gill S. A process for the step-by-step integration of differential equations in an automatic digital computing machine. Proc Camb Philos Soc 1951;47:96–108.
[17] Vafai K, Alkire RL, Tien CL. An experimental investigation of heat transfer in variable porosity media. ASME J Heat Transfer 1985;107:642–7.
[18] Tien CL, Hong JT. Natural convection in porous media under non-Darcian and non-uniform permeability conditions. In: Kakac, et al., editors. Natural convection. Washington, DC: Hemisphere; 1985.
[19] Fathalah FA, Elsayed MM. Natural convection due to solar radiation over a non absorbing plate with and without heat losses. Int J Heat Fluid Flow 1980;2:41–5.

[20] Oztop HF, Abu-Nada E. Numerical study of natural convection in partially heated rectangular enclosures filled with nanofluids. Int J Heat Fluid Flow 2008;29:1326–36.
[21] Sparrow EM, Cess RD. Radiation heat transfer. Washington: Hemisphere; 1978.
[22] Sattar MA. Local similarity transformation for the unsteady two-dimensional hydrodynamic boundary layer equations of a flow past a wedge. Int J Appl Math Mech 2011;7:15–28.
[23] Aminossadati AM, Ghasemi B. Natural convection cooling of a localized heat source at the bottom of a nanofluid-filled enclosure. Eur J Mech B/Fluids 2009;28:630–40.
[24] Maxwell JC. A treatise on electricity and magnetism. 2 unabridged 3rd ed. Oxford, UK: Clarendon Press; 1891.
[25] Schlichting H. Boundary layer theory. New York: McGraw Hill Inc.; 1979.
[26] White FM. Viscous fluid flows. 3rd ed. New York: McGraw-Hill; 2006.
[27] Akhavan-Behabadi MA, Fakoor Pakdaman M, Ghazvini M. Experimental investigation on the convective heat transfer of nanofluid flow inside vertical helically coiled tubes under uniform wall temperature condition. Int Commun Heat Mass Transfer 2012;39:556–64.

Nomenclature

B_0: magnetic field strength
C: nanoparticles volume fraction
C_w: nanoparticle volume fraction at the wall
C_∞: ambient nanoparticle volume fraction
c_p: specific heat at constant pressure
C_T: temperature ratio
Ec: Eckert number
f: dimensionless stream function
F: empirical constant in the second-order resistance
F_n: Forchheimer number
g: acceleration due to gravity
k: thermal conductive
k^*: mean absorption coefficient
K: permeability of the porous medium
M: magnetic parameter
N: conductive radiation parameter
Pr_f: Prandtl number
q''_{rad}: incident radiation flux of intensity
S: suction/injection parameter
T: temperature of the fluid
T_w: temperature at the wall
T_∞: ambient temperature
u, v: velocity components along x- and y-axes
$U(x)$: uniform velocity of the free stream flow
v_0: velocity of suction/injection

Greek symbols

α_{f_n}: thermal diffusivity of the nanofluid
β: coefficient of thermal expansion
θ: dimensionless temperature
ϕ: dimensionless nanoparticle volume fraction
η: similarity variable
μ: dynamic viscosity
μ_{f_n}: effective dynamic viscosity of the nanofluid
σ: electric conductivity of the fluid
σ_1: Stefan–Boltzman constant
ρ_f: density of the base fluid
ρ_{f_n}: effective density of the nanofluid
$(\rho c)_f$: heat capacity of the base fluid
$(\rho c)_p$: effective heat capacity of the nanoparticle material
ν: kinematic viscosity
ψ: stream function
σ_1: Stefan–Boltzman constant
Ω: angle of the wedge